phase, despite the apparent correct band filling and suitable interfullerene spacing. It appears that the orientational state of the fullerenes and the intercalate-carbon interaction subtly control the pair-binding mechanism in the fullerides.

REFERENCES AND NOTES

1. P. W. Stephens et al., Nature 351, 632 (1991).
2. K. Prassides et al., Science 263, 950 (1994).
3. K. Kniaz et al., Solid State Commun. 88, 47 (1993).
4. S. Chakravarty, M. P. Gelfand, S. Kivelson, Science 254, 970 (1991).
5. C. M. Varma et al., ibid., p. 989; M. Schluter et al., Phys. Rev. Lett. 68, 526 (1992); I. I. Mazin et al., Phys. Rev. B 45, 5114 (1992).
6. R. M. Fleming et al., Nature 352, 787 (1991).
7. S. Satpathy et al., Phys. Rev. B 46, 1773 (1992); M. P. Gelfand and J. P. Lu, ibid., p. 4367; Appl. Phys. A 56, 215 (1993); T. Yildirim, S. Hong, A. B. Harris, E. J. Mele, Phys. Rev. B 48, 12262 (1993); R. P. Gupta and M. Gupta, ibid. 47, 11635 (1993).
8. K. Tanigaki et al., Europhys. Lett. 23, 57 (1993).
9. P. C. Chow et al., Phys. Rev. Lett. 69, 2943 (1992).
10. W. N. Setzer and P. von R. Schleyer, Adv. Organomet. Chem. 24, 553 (1985).
11. J. E. Fischer, in Intercalated Layered Materials, F. Lévy, Ed. (Reidel, Dordrecht, Netherlands, 1979), pp. 481–532.
12. Li_2CsC_{60} samples were synthesized by direct reaction between C_{60} and alkali metals. Stoichiometric amounts of C_{60}, Li, and Cs were introduced into tantalum cells that were sealed in pyrex glass tubes filled with helium to 500 torr. These tubes were heated at 230°C for 12 to 24 hours and then baked at 430°C for 2 to 3 weeks. Susceptibility measurements were performed to 50 mK with a dilution refrigerator. DSC measurements were performed with a Mettler (Hightstown, NJ) DSC 3000 calorimeter on 10 to 30 mg of sample, sealed in aluminum pans. Measurements were carried out in the temperature range of 100 to 450 K at rates of 5 and 10 K/min.
13. PROFIL, 5.12; J. K. Cockcroft, Birkbeck College, London.
14. K. Tanigaki et al., Phys. Rev. B, in press.
15. H. B. Bürgi, R. Restori, D. Schwarzenback, Acta Crystallogr. B 49, 832 (1993); K. Rapcewicz and J. Przystawa, Phys. Rev. B, in press.
16. W. Press and A. Hüller, Acta Crystallogr. A 29, 252 (1973); J. P. Amoureux and M. Bee, Acta Crystallogr. B 36, 2636 (1980); J. K. Cockcroft and A. N. Fitch, Z. Kristallogr. 184, 123 (1988).
17. For spherical-shell scatterers, the structure factor is the Fourier transform of the convolution of the position of the center of the shell, R, the scattering density function ρ(r) of the shell (with the origin for r at R), and its thermal motion, μ.

$$F_{hkl} = F^{rot}(Q)exp(i\mathbf{Q} \cdot \mathbf{R}) \cdot exp[-W(\mathbf{Q})] \quad (1)$$

where **Q** is the scattering vector, $W(\mathbf{Q})$ is the Debye-Wallerfactor, and the rotational form factor of the shell is given by

$$F^{rot}(Q) = \int_{unit\ cell} f(Q) exp(i\mathbf{Q} \cdot \mathbf{R}) \cdot \rho(\mathbf{r}) dr \quad (2)$$

where $f(Q)$ is the atomics scattering factor. The orientational scattering density, ρ(**r**), is expressed in terms of the SASH functions $[K_{l\nu}(\theta,\phi)]$ obtained from linear combinations of spherical-harmonic functions $\{Y_{lm}(\theta,\phi)$ [F. C. von der Lage and H. A. Bethe, Phys. Rev. 71, 612 (1947)]}, as

$$\rho(\mathbf{r}) = \sum_l \sum_\nu C_{l\nu} K_{l\nu}(\theta_r,\phi_r) \delta(r - R)/4\pi R^2 \quad (3)$$

where R is the radius of the shell and $C_{l\nu}$ are refinable coefficients. Substitution into Eq.2 and use of the orthonormality of the SASH functions results in

$$F^{rot}(Q) = (4\pi)^{1/2} f_C(Q) \sum_l \sum_\nu i^l j_l(QR) C_{l\nu} K_{l\nu}(\theta_Q,\phi_Q) \quad (4)$$

where $j_l(QR)$ are the l-th order spherical Bessel functions and $f_C(Q)$ is the carbon scattering factor. Only the coefficients, $C_{l\nu}$, that transform as the totally symmetric representation of the point group of the site symmetry of the shell of atoms are nonzero. The integer ν labels the particular representation within A_{lg} for a given value of l.

18. K. H. Michel, J. R. D. Copley, D. A. Neumann, Phys. Rev. Lett. 68, 2929 (1992).
19. I. Hirosawa, J. Mizuki, K. Tanigaki, H. Kimura, Solid State Commun. 89, 55 (1994).
20. We tested our procedure by refining a room temperature synchrotron x-ray diffraction profile of pristine C_{60}, collected at Brookhaven National Laboratory. Reliable cubic harmonic $C_{6,1}$ and $C_{10,1}$ coefficients were routinely extracted from the refinement and were in good agreement with the values deduced by Chow et al., (9) from single-crystal data. We thank P. A. Heiney for making his raw data available to us [J. Phys. Chem. Solids 53, 1333 (1992)].
21. T. Yildirim et al., Phys. Rev. Lett. 71, 1383 (1993).
22. C. Christides et al., Europhys. Lett. 24, 755 (1993).
23. We thank the Engineering and Physical Sciences Research Council, United Kingdom, for financial support and access to Daresbury Laboratory, and K. H. Michel for useful discussions. M.G. is a participant of the University of Sussex–University of Waterloo (Canada) student exchange programme.

Critical Behavior in the Satisfiability of Random Boolean Expressions

Scott Kirkpatrick and Bart Selman

Determining the satisfiability of randomly generated Boolean expressions with k variables per clause is a popular test for the performance of search algorithms in artificial intelligence and computer science. It is known that for $k = 2$, formulas are almost always satisfiable when the ratio of clauses to variables is less than 1; for ratios larger than 1, the formulas are almost never satisfiable. Similar sharp threshold behavior is observed for higher values of k. Finite-size scaling, a method from statistical physics, can be used to characterize size-dependent effects near the threshold. A relationship can be drawn between thresholds and computational complexity.

Properties of randomly generated combinatorial structures often exhibit sharp threshold phenomena. A good example can be found in random graphs. A graph is defined as a set of points (vertices) in space with lines (edges) connecting pairs of vertices. A random graph is generated by randomly selecting pairs of vertices to be connected by edges. Erdös and Rényi (1) showed that many properties of random graphs can be predicted with a very high accuracy. Consider the sizes of connected clusters. A connected cluster is a group of vertices where, starting at an arbitrary vertex, one can reach any other vertex in the group by traversing one or more edges in the graph. It is intuitively clear that the more edges in the graph, the more vertices will be interconnected and the larger the clusters will be. What is surprising is that gradually increasing connectivity leads to sudden changes in the distribution of cluster sizes.

Let N be the number of vertices and M be the number of edges. If we make N and M large but hold their ratio $\alpha \equiv M/N$ constant, then we can identify two regimes: When $\alpha < 1/2$, many small isolated clusters of maximum size $\ln N$ are found; when $\alpha >$

S. Kirkpatrick, IBM Thomas J. Watson Research Center, Yorktown Heights, NY 10598, USA. E-mail: kirk@watson.ibm.com
B. Selman, AT&T Bell Laboratories, Murray Hill, NJ 07974, USA. E-mail: selman@research.att.com

$1/2$, a single giant component with size proportional to N absorbs many of the clusters. At the boundary between the two regimes, when α has its critical value $\alpha_c = 1/2$, the largest clusters are proportional to $N^{2/3}$. Subsequent work (2, 3) has made precise the sharpness of the threshold: Its characteristics persist across a range of α of order $N^{-1/3}$ about $\alpha_c = 1/2$. This is now recognized as the prototype of "percolation" phase transitions studied in simple models of real inhomogeneous materials, which change sharply from nonconducting to conducting on macroscopic scales as a local measure of connectedness increases (4). We shall use this well-understood model to test techniques for the identification of critical phenomena in less understood combinatoric structures.

Threshold phenomena have recently been observed in randomly generated Boolean expressions or formulas. Mitchell et al. (5) considered the k-satisfiability problem (k-SAT). An instance of k-SAT is a Boolean formula in a special form, called conjunctive normal form (CNF). An example of such a formula is $(x \lor y) \land (\bar{x} \lor \bar{y}) \land (x \lor \bar{y})$, where x and y are Boolean variables and $\land$, $\lor$, and the overbar are logical operators denoting, respectively, AND, OR, and NOT.

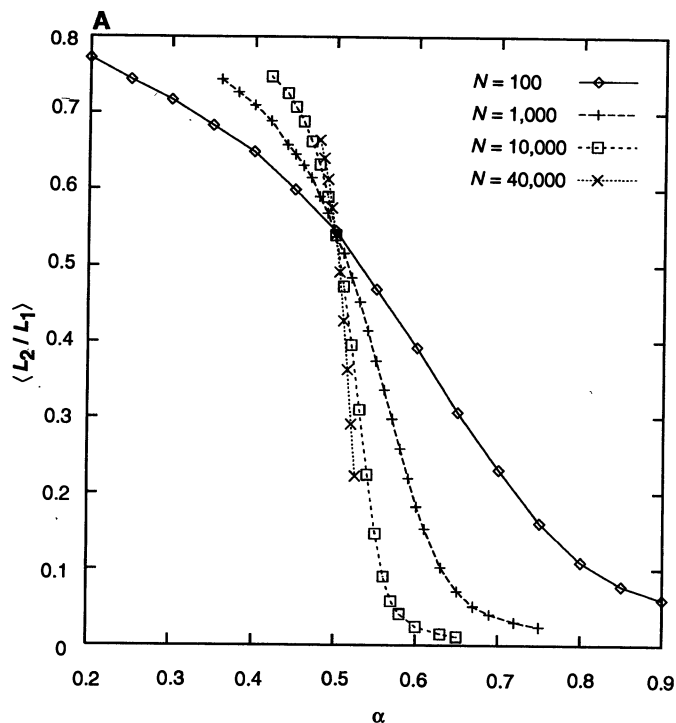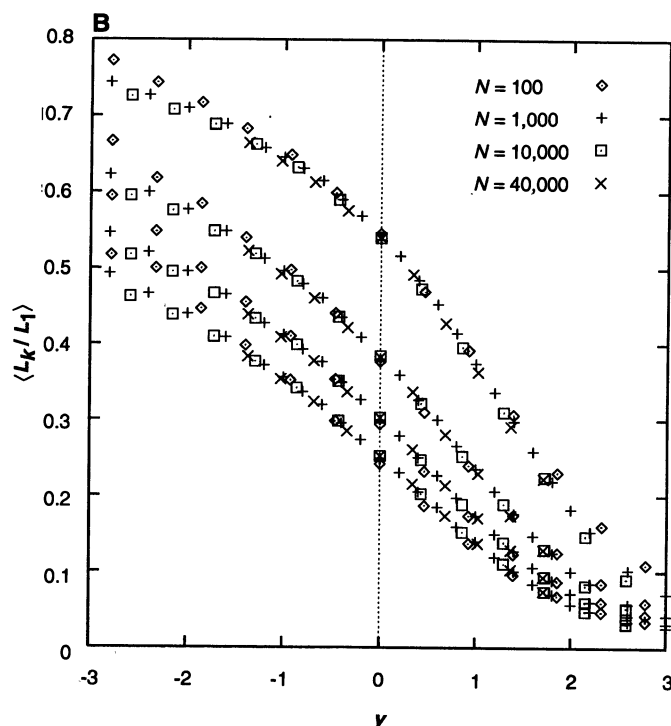Each Boolean variable can be assigned either true or false. Depending on the

Fig. 1. (A) The ratio of the size of the second largest cluster to that of the largest cluster plotted against α for several values of N. We analyzed 10,000 samples for each data point, giving roughly 1% accuracy through-

out. **(B)** Rescaled cluster data (from top to bottom, the curves correspond to $k = 2$ to 5).

values assigned to the variables, the formula as a whole evaluates to either true or false. For example, if we assign x to true and y to false, each clause, and therefore our whole formula, evaluates to true. Each disjunction (logical OR), such as $(x \lor \bar{y})$, is called a clause. A k-CNF formula consists of a collection of such clauses, each containing k variables, joined by conjunctions (logical ANDs). We use N to denote the total number of Boolean variables, and M the number of clauses. So, our example formula has $k = 2$, $N = 2$, and $M = 3$. In a randomly generated formula, each clause is generated by randomly selecting k distinct variables from the set of N variables or their negations (logical NOT). The problem is to determine whether there is an assignment to the variables such that all clauses evaluate to true, in which case the formula is called satisfiable. The values of M, N, and their ratio α define the scale and natural parameters of this problem just as in the random graph model.

For randomly generated 2-SAT instances, it has been shown analytically that for large N, when the ratio $\alpha < 1$, the instances are almost all satisfiable, whereas for $\alpha > 1$, almost all instances are unsatisfiable (6, 7). For $k \geq 3$, a rigorous analysis has proven to be elusive. Loose upper and lower bounds have been obtained, but there is yet no rigorous proof of the existence of a threshold (8). Experimental evidence, however, strongly suggests a threshold with $\alpha \approx 4.2$ for 3-SAT (5, 9, 10).

One of the main reasons for studying randomly generated CNF formulas is for their use in the empirical evaluation of combinatorial search algorithms (10–12). Formulas with $k = 3$ (3-CNF) are good candidates for the evaluation of such algorithms because determining their satisfiability is an NP-complete problem (13), a member of a class of problems that can easily be transformed into one another yet for which no efficient (polynomial time, rather than exponential) algorithm for their exact solution is known. For $k > 3$, k-SAT remains NP-complete. For $k = 1$ or 2, the satisfiability problem can be solved efficiently (14).

One has to be careful in the use of randomly generated formulas: Simple heuris-

tic methods can often quite easily determine the satisfiability of most such formulas. This has led to some overly strong claims in the literature about the handling of very large formulas. Computationally challenging test instances can be obtained with high probability by generating formulas at or near the threshold (5). Cheeseman et al. (15) made a similar observation of increased computational cost for heuristic search at a boundary between two distinct phases or behaviors of a combinatorial model.

We provide here a precise characterization of the dependence on N of the threshold phenomena for k-SAT with k ranging from 2 to 6. Our analysis shows that the threshold in k-SAT closely resembles the
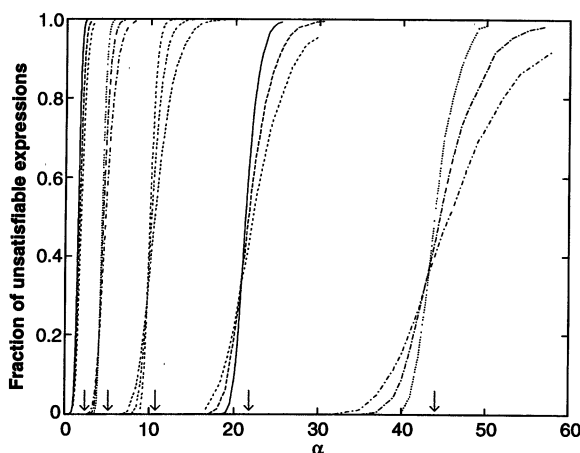

Fig. 2. Fraction of unsatisfiable Boolean expressions for k-SAT (from left to right, the groups of curves correspond to $k = 2$ to 6) for N from 12 to 50, typically averaged over 10,000 samples for roughly 1% accuracy. The curves sharpen up with increasing N at each k. Values of N were (for $k = 2$ through 4) 12, 24, and 50; (for $k = 5$ and 6) 12, 20, and 40. The arrows mark α_{ann}.
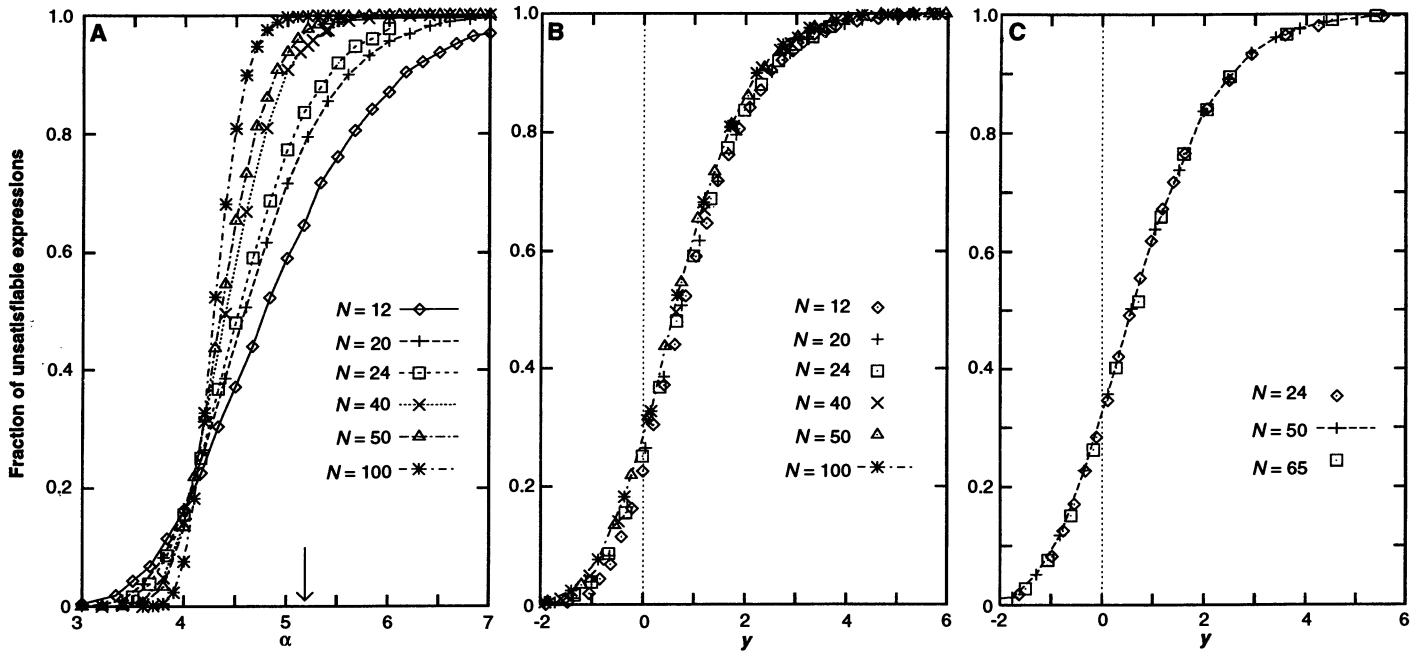
Fig. 3. (**A**) Threshold data for 3-SAT, $N = 12$ to 100. Arrow marks α_{ann}. Both the threshold shift and the increasing slope in the curves can be accounted for by finite-size scaling. (**B**) Rescaled 3-SAT data with $\alpha_c = 4.17$ and $v = 1.5$, which are determined from experimental data (first, α_c is determined as the crossing point of the curves at large N, and then v is chosen to make the slopes match up though the critical region). (**C**) Rescaled 4-SAT data with $\alpha_c = 9.75$ and $v = 1.25$ lead to a tighter fit to a single curve. The critical parameters from this analysis are given in Table 1.

phase transition studied in spin glasses (16). We use finite-size scaling (4, 17), a method from statistical physics in which the observation of how the width of a transition narrows with increasing sample size gives direct evidence for critical behavior at a phase transition. We first illustrate the finite-size scaling approach on random graphs.

The empirical observation behind phenomenological scaling is that sufficiently close to a threshold or critical point, systems of all sizes are indistinguishable except for an overall change of scale. In the random graph ensemble, the clusters of size $N^{2/3}$ that occur close to its threshold in a random graph with $N = 100$ should simply look like coarse versions of the clusters found in a graph with $N = 10,000$. However, to make the comparison, the narrow threshold observed for very large graphs must be expanded in scale to compare it with the broader threshold seen in small graphs. In the random graph ensemble, we know exactly how to do this. Correcting for the known $N^{-1/3}$ dependence of the width and normalizing α to its threshold value α_c, we define a rescaled parameter $y \equiv N^{1/3}2(\alpha - 1/2)$ against which to plot data for a graphical analysis.

But what to plot? A well-behaved quantity for this problem proves to be the sizes of the larger clusters, normalized to the size of the largest cluster in the same graph. When α is small, all clusters should be of the same general magnitude, so these ratios tend to unity. For $\alpha \gg 1/2$, normalization by the size of the giant cluster makes all the ratios

tend to zero. Let L_k denote the size of the k-th largest cluster found in a particular graph, and $\langle \rangle$ represent averaging over many samples of graphs with the same M and N. Curves of $\langle L_2/L_1 \rangle$ plotted against α (Fig. 1A) show the sharpening of the transition with increasing N, and all intersect at the critical point $\alpha = 1/2$. Plotting them against y (Fig. 1B), we find that the averaged normalized cluster sizes follow universal forms through the critical regions, only separating when $|y| > 1$. The values of the size ratios at the critical point are insensitive to N: They are $\langle L_2/L_1 \rangle = 0.538 \pm 0.0015$, $\langle L_3/L_1 \rangle = 0.382 \pm 0.001$, $\langle L_4/L_1 \rangle = 0.302 \pm 0.0006$, and $\langle L_5/L_1 \rangle = 0.252 \pm 0.0006$ (averaged over 160,000 samples at each N).

It is surprising that finite-size scaling works here because the standard heuristic derivations (4, 17) explain the size dependence of a crossover between two phases as a measurement of a correlation length ξ, which diverges at the critical point in an infinite system. If two points in such a system are separated by more than ξ, they are independent. Combinatoric problems like the random graph ensemble have no lengths, and there is no geometric criterion for separating them into independent subproblems. Yet it appears that power-law behavior in the size N replaces scaling with respect to a length. This is consistent with renormalization-group derivations of finite-size scaling (18), in which lengths occur only through the volume of the system, measured here by N.

Table 1. Critical parameters for random k-SAT. The errors show the range of each parameter over which the best fits were obtained.

k	α_{ann}	α_c	y_{50}	v
2	2.41	1.0	2.25	2.6 $\pm$ 0.2
3	5.19	4.17 $\pm$ 0.05	0.74	1.5 $\pm$ 0.1
4	10.74	9.75 $\pm$ 0.05	0.67	1.25 $\pm$ 0.05
5	21.83	20.9 $\pm$ 0.1	0.71	1.10 $\pm$ 0.05
6	44.01	43.2 $\pm$ 0.2	0.69	1.05 $\pm$ 0.05

We now apply the rescaling procedure to k-SAT, determining the critical concentration by exact calculation if possible, by observation of the measured properties if not. For example, the intersection of all the lines in Fig. 1A identifies the critical point even if it were not known to be 1/2.

We generated extensive data on the satisfiability of randomly generated k-CNF expressions with k ranging from 2 to 6 and determined the fraction of expressions that is unsatisfiable as a function of α (Fig. 2). We used a highly optimized implementation (9) of the Davis-Putnam procedure (19). This procedure performs a backtrack search through the space of possible truth assignments and is the fastest known complete procedure for satisfiability testing on many classes of formulas (20).

Figure 2 shows a clear threshold for each value of k. Except for the case $k = 2$, the curves cross at a single point and sharpen up with increasing N. For $k = 2$, the intersections between the curves for the largest

values of N seem to converge to a single point as well, although the curves for smaller N deviate. The thresholds move rapidly to the right with increasing k. This is because a clause with k distinct variables prohibits only one of the 2^k truth assignments to the k variables, and thus, the constraints get weaker as k increases.

We can estimate the behavior of the threshold and crossover for large values of k by neglecting the overlap between clauses. This is called an annealed estimate, by analogy with annealed theories of materials (16), which average independently over sources of disorder. Each of the M clauses reduces the expected number of satisfying variable assignments from 2^N by a factor of $(2^k - 1)/(2^k) = (1 - 2^{-k}) \equiv \gamma_k$. We get a plausible estimate for the threshold by asking when, on average, only one satisfying assignment survives. If $2^N \gamma_k^M = 2^{N(1 + \alpha \log_2 \gamma_k)} = 1$, then $\alpha_{ann} = -1/\log_2 \gamma_k \approx 2^k \ln 2$. The annealed estimate α_{ann} is identical to the upper bound described in (6). See Table 1 for values of α_{ann}.

The annealed estimate can be extended (21) to describe the crossover for large k. We estimate the probability that there are no satisfying configurations as $(1 - \gamma_k^{\alpha N})^{2^N}$. This can be transformed into

$$[1 - 2^{-N(\alpha/\alpha_{ann})}]^{2^N}$$

$$= [1 - 2^{-N(\alpha - \alpha_{ann})/\alpha_{ann}}/2^N]^{2^N}$$

$$\approx e^{-2^{-y_{ann}}}$$

where

$$y_{ann} = N(\alpha - \alpha_{ann})/\alpha_{ann}$$

The extension of this to finite-size (4, 17) scaling is just

$$y = N^{1/\nu}(\alpha - \alpha_c)/\alpha_c$$

Figure 3A shows the threshold in more detail for several values of N for random 3-CNF formulas. Rescaling with $\alpha_c = 4.17$ and $\nu = 1.5$ (Fig. 3B), we find that these two parameters capture both the threshold shift and the steepening of the curves. Rescaling the data for random 4-SAT (Fig. 3C) leads to a tighter fit to a single curve. In Table 1 we give the critical parameters obtained from this analysis for k from 2 to 6: ν tends to 1, the annealed value, and α_{ann} becomes an increasingly good approximation to α_c as k increases.

The rescaled curves in Fig. 3, B and C, are similar in form. Combining the rescaled curves for all values of k (Fig. 4), we find that the curves for $k \geq 3$ all roughly coincide. As $k \to \infty$, the curves approach the annealed limit derived above. The curve for $k = 2$ is also similar but shifted to the right from the others.

From the perspective of performance evaluation for search algorithms, the point where 50% of the formulas are unsatisfiable is thought to be where the computationally hardest problems are found (5, 15). Note that the 50% point lies somewhat to the right of the scale-invariant point (the point where the curves cross each other in Figs. 2

and 3A) and shifts with N. Because the fraction of unsatisfiable formulas is given by the rescaled function $f_k(y)$ (Fig. 4), a description of the 50% threshold shift follows immediately. If we define y_{50} by $f_k(y_{50}) = 0.5$, then $\alpha_{50} = \alpha_c(1 + y_{50}N^{-1/\nu})$. For $k = 3$, $\alpha_{50} \approx 4.17 + 3.1N^{-2/3}$ (Fig. 3B and Table 1). Crawford and Auton (9) fit their data on the 50% point as a function of N by arbitrarily assuming that the leading correction will be $O(1/N)$. They obtained $\alpha_{50} = 4.24 + 6/N$. The two expressions differ by only a few percent as N ranges from 10 to ∞, but our procedure fits better away from α_{50}. For $k = 2$, the difference between the scaling expression and a $1/N$ extrapolation will be greater. Given the good fit of our scaling analysis, we conjecture that this method can also be of use in the characterization of phase transitions in other combinatorial problems of interest.

Physicists have speculated that characteristics that lead to interesting critical phenomena in random systems are at the root of computational complexity and NP-completeness. Huberman and colleagues (22) have focused on the diverging correlation length seen at continuous phase transitions as the root of computational complexity. This is consistent with the fact that computationally hard instances of problems such as graph coloring and 3-SAT are densest at or near phase transitions (5, 15). Yet there are other NP-complete problems (for example, the traveling salesman or max-clique) that lack a clear phase boundary at which "hard problems" cluster. Percolation thresholds are phase transitions with diverging correlations, yet the cost of finding the largest cluster never exceeds N steps. Thus, diverging correlations alone do not cause exponential complexity.

Fu and Anderson (23) had earlier proposed spin glasses (magnets with two-spin interactions of random sign) as having inherent exponential complexity. Models of spin glasses are known to possess many low-lying near-optimal states of no obvious symmetry and are nonergodic, that is, the shortest paths between these states can be arbitrarily long if one moves by the typical methods of local rearrangement search. Real spin glass materials exhibit very long magnetic relaxation times, presumably because of this nonergodicity.

In fact, both random signs and correlations are important factors in computational complexity but do not necessarily imply NP-completeness, which is somewhat special. In 2-SAT, which has random phases, finding a satisfying assignment, or proving its nonexistence, can be done in linear time by a technique pointed out by Aspvall et al. (14). The spin glass Hamiltonians studied in (23) are similar to our 2-SAT formulas, but the questions studied are different and
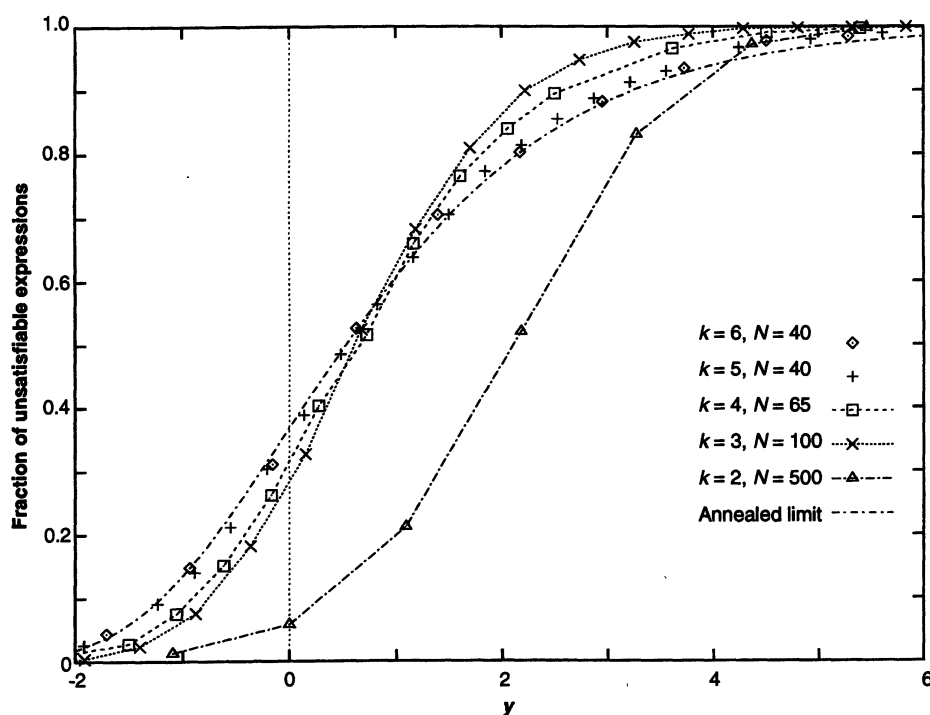

Fig. 4. Rescaled crossover functions for $k = 2$ through 6. The fraction of unsatisfiable formulas is given by the invariant function $f_k(y)$.

computationally much harder. Finding an assignment that falsifies the minimum number of clauses is like finding the ground state in a spin glass phase and does not reduce to a single search on the directed graph of (14). For 2-SAT, in fact, finding such "ground states" is NP-hard (13). Therefore, if both diverging correlations (diverging in size if no lengths are defined) and a "spin glass" phase occur, we expect search to be exponentially difficult.

REFERENCES AND NOTES

1. P. Erdös and A. Rényi, Publ. Math. Inst. Hung. Acad. Sci. 5, 17 (1960).
2. B. Bollobás, Random Graphs (Academic Press, London, 1985); J. Spencer, Ten Lectures on the Probabilistic Method (Society for Industrial and Applied Mathematics, Philadelphia, PA, 1987).
3. S. Janson, D. E. Knuth, T. Łuczak, B. Pittel, Random Struct. Algorithms 4, 231 (1993).
4. D. Stauffer and A. Aharony, Introduction to Percolation Theory (Taylor and Francis, London, 1992).
5. D. Mitchell, B. Selman, H. J. Levesque, in Proceedings of the 10th National Conference on Artificial Intelligence (AAAI Press, Menlo Park, CA, 1992), p. 459; extended version in Artif. Intell., in press.
6. V. Chvátal and B. Reed, in Proceedings of the 33rd Annual Symposium on Foundations of Computer Science (IEEE Society Press, Los Alamitos, CA, 1992), p. 620.
7. A. Goerdt, in Proceedings of the 17th International Symposium on the Mathematical Foundation of Computer Science, I. M. Havel and V. Koubek, Eds. (Springer-Verlag, Berlin, 1990), p. 264.
8. A. Z. Broder, A. M. Frieze, E. Upfal, in Proceedings of the 4th Annual ACM-SIAM Symposium on Discrete Algorithms (Society for Industrial and Applied Mathematics, Philadelphia, PA, 1993), p. 322.
9. J. M. Crawford and L. D. Auton, in Proceedings of the 11th National Conference on Artificial Intelligence (AAAI Press, Menlo Park, CA, 1993), p. 21.
10. T. Larrabee and Y. Tsuji, in Proceedings of the AAAI Symposium on Artificial Intelligence and NP-Hard Problems (1993), p. 112.
11. B. Selman, H. J. Levesque, D. Mitchell, in (5), p. 440.
12. A. P. Kamath et al., Ann. Oper. Res. 25, 43 (1990).
13. S. A. Cook, Proceedings of the 3rd Annual ACM Symposium on Theory of Computing (Association for Computing Machinery, New York, 1971), p. 151.
14. B. Aspvall, M. F. Plass, R. E. Tarjan, Inf. Process. Lett. 8, 121 (1979).
15. P. Cheeseman, B. Kanefsky, W. M. Taylor, in Proceedings of the 12th International Conference on Artificial Intelligence, R. Reiter and J. Mylopoulos, Eds. (Morgan Kaufmann, San Mateo, CA, 1991), p. 331.
16. M. Mézard, G. Parisi, M. A. Virasoro, Spin Glass Theory and Beyond (World Scientific, Singapore, 1986).
17. S. Kirkpatrick and R. H. Swendsen, Commun. ACM 28, 363 (1985).
18. M. N. Barber, in Phase Transitions and Critical Phenomena, C. Domb and J. L. Lebowitz, Eds. (Academic Press, London, 1983), vol. 8, p. 145.
19. M. Davis and H. Putnam, J. Assoc. Comput. Mach. 7, 201 (1960).
20. O. Dubois, P. Andre, Y. Boufkhad, J. Carlier, in Proceedings of the 2nd DIMACS Implementation Challenge (American Mathematical Society, Providence, RI, in press).
21. S. Kirkpatrick, G. Györgyi, N. Tishby, L. Troyansky, in Advances in Neural Information Processing Systems, vol. 6, J. Cowan, G. Tesauro, J. Alspector, Eds., in press; and unpublished results.
22. S. H. Clearwater, B. A. Huberman, T. Hogg, Science 254, 1181 (1991).
23. Y. Fu, in Lectures in the Sciences of Complexity,

D. Stein, Ed. (Addison-Wesley, Reading, MA, 1989), p. 815.
24. This work was done during S.K.'s 1993 sabbatical at the Racah Institute of Physics and Center for Neural Computation, Hebrew University, Jerusa-

Langmuir-Blodgett Films of a Functionalized Molecule with Cross-Sectional Mismatch Between Head and Tail

J. Garnaes, N. B. Larsen, T. Bjørnholm,* M. Jørgensen, K. Kjaer, J. Als-Nielsen, J. F. Jørgensen, J. A. Zasadzinski

A functionalized surfactant has been investigated as floating monolayers by synchrotron x-ray diffraction and as bilayers transferred to solid supports by the Langmuir-Blodgett technique through atomic force microscopy. The transfer process is accompanied by an increase of the unit cell area (about 17 percent) and by an increase of the average domain diameter of nanometer-scale domains (about three times). The unit cell area of the floating monolayer corresponds to close packing of the head groups and a noncharacteristic packing of the tilted alkyl chains. The larger unit cell area of the bilayer film is consistent with a particular ordered packing of the alkyl chains, leaving free space for the head groups.

As a means of organizing complex molecules, the Langmuir-Blodgett (LB) technique (1) has many potential applications within molecular electronics, nonlinear optics, and conducting thin films (Fig. 1). In this context, the structural properties of the LB films may have important consequences for applications; for example, the number of defects may limit electrical contact, while the degree of order and the sizes of domains may limit, for example, the conductivity. In addition, changes of these properties may occur when the floating monolayers are transferred to solid substrates. By the combination of x-ray diffraction (XRD) of floating monolayers with atomic force microscopy (AFM) of films transferred to solid supports, it is possible to reveal these features.

Because molecules with relatively large head groups, compared to alkyl chains, are often used in functionalized LB films (Fig. 1), the design of the functional organic molecules requires an understanding of the packing properties of molecules with a "cross-sectional mismatch" between head and tail groups. As an example of such a molecule, we present a structural study performed of both a floating monolayer and a bilayer transferred to a solid substrate.

The particular molecule in question is an electron acceptor, octadecylthio-1,4-benzoquinone (Fig. 1E), which forms nonlinear optical films when interfaced with electron donor molecules (2, 3).

Previous comparative studies of floating monolayers and transferred multilayers have focused on fatty acids and similar types of compounds that have head and tail groups of similar cross-sectional size. Such compounds have been extensively studied by XRD in situ at the water surface (4–9) and by AFM (10–13) and electron diffraction (14) as transferred multilayers. These studies have in many cases revealed highly
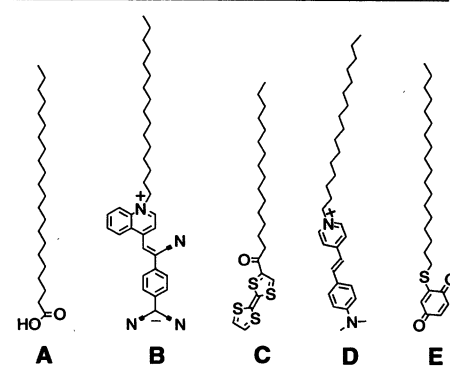
J. Garnaes and J. F. Jørgensen, Danish Institute of Fundamental Metrology, Lundtoftevej 100, DK-2800 Lyngby, Denmark.
N. B. Larsen, T. Bjørnholm, M. Jørgensen, Centre for Interdisciplinary Studies of Molecular Interactions, Department of Chemistry, University of Copenhagen, Fruebjergvej 3, DK-2100 Copenhagen, Denmark.
K. Kjaer and J. Als-Nielsen, Physics Department, Risø National Laboratory, DK-4000 Roskilde, Denmark.
J. A. Zasadzinski, Department of Chemical and Nuclear Engineering, University of California, Santa Barbara, CA 93106, USA.

*To whom correspondence should be addressed.

Fig. 1. Molecules used in LB films in different areas of research. (**A**) Fatty acids (26) have been the prototype for structural studies of LB films. Opposed to fatty acids, a large head group is common for electronically active molecules. The functionalized molecules given in this table have been used for (**B**) electrical rectification (27), (**C**) conduction/redox activity (28), (**D**) nonlinear optics (29), and (**E**) redox activity such as electron acceptor (2, 3, 20).